Mon. Not. R. Astron. Soc. **000**, 000–000 (0000) Printed 5 February 2008 (MN LATEX style file v2.2)

The polarisation signature from microlensing of circumstellar envelopes in caustic crossing events

R. Ignace[1,2], J. E. Bjorkman[3], and H. M. Bryce[1,4]
[1] *Department of Astronomy, University of Wisconsin, 475 North Charter Street, Madison, WI 53706, USA*
[2] *Department of Physics, Astronomy, & Geology, East Tennessee State University, Johnson City, TN 37614, USA*
[3] *Ritter Observatory, Department of Physics and Astronomy, University of Toledo, Toledo, OH 43606, USA*
[4] *Department of Physics and Astronomy, University of Glasgow, Glasgow, Scotland, UK*

5 February 2008

ABSTRACT

In recent years it has been shown that microlensing is a powerful tool for examining the atmospheres of stars in the Galactic Bulge and Magellanic Clouds. The high gradient of magnification across the source during both small impact parameter events and caustic crossings offers a unique opportunity for determining the surface brightness profile of the source. Furthermore, models indicate that these events can also provide an appreciable polarisation signal – arising from differential magnification across the otherwise symmetric source. Earlier work has addressed the signal from a scattering photosphere for both point mass lenses and caustic crossings. In a previous paper, polarimetric variations from point lensing of a circumstellar envelope were considered, as would be suitable for an extended envelope around a red giant. In this work we examine the polarisation in the context of caustic crossing events, the scenario which represents the most easily accessible situation for actually observing a polarisation signal in Galactic microlensing. Furthermore we present an analysis of the effectiveness of using the polarimetric data to determine the envelope properties, illustrating the potential of employing polarimetry in addition to photometry and spectroscopy with microlensing follow-up campaigns.

Key words: polarisation –gravitational lensing – stars: atmospheres

1 INTRODUCTION

Much attention has been paid to the situation in which the analytic case of the magnification of a point source by a point lens breaks down. It has been noted that for small lens–source separations, the finite size of the source star needs to be considered (Nemiroff & Wickramasinghe 1994; Witt & Mao 1994; Witt 1995; Peng 1997). Such events not only constrain the lens properties by breaking the degeneracy in the event parameters (Gould 1994) but also provide valuable stellar atmosphere information, such as limb darkening (Valls-Gabaud 1998; Hendry et al. 1998), polarisation (Simmons et al. 1995a,b; Newsam et al. 1998), motions in circumstellar envelopes (Ignace & Hendry 1999) and the presence of starspots (Heyrovský & Sasselov 2000). The opportunity for studying stellar atmospheres through microlensing as described in Sackett (2001) and Gould (2001) has clear advantages over other methods such as eclipsing binaries, because the source and means of studying the source are not coupled and the flux from the source is magnified rather than diminished.

Binary lenses produce another deviation from a standard microlensing lightcurve, because caustics are produced (e.g., Schneider & Weiss 1986). It is the high gradient of magnification across the caustic that allows one to infer information about the source intensity profile, even though the source images are not individually resolvable with current instruments. Despite binary lens events only accounting for about 5% of microlensing events (e.g., Alcock *et al.* 2000), it is more likely that finite source effects will be relevant for a binary lens rather than a point lens. The reason is that finite source effects are mainly discernible only when the lens transits the source itself (Gould 1994). Since the angular Einstein radius $\theta_{\rm E}$ (see Eq. 3) is usually much larger than the angular source size, such transits tend to be rare. On the other hand, the caustic structures giving rise to high magnifications in binary lens events

are spatially extended (of order $\theta_{\rm E}$ in scale), and so caustic crossings by the more distant source are relatively common in events associated with binary lenses. So it is more expedient to study the resolution of stellar atmospheres due to binary lenses than point lenses. The structure of the caustics produced and the resulting magnification and lightcurves from binary microlenses has been discussed extensively in the literature (Mao & Paczyński 1991; Mao & Di Stefano 1995; Di Stefano & Perna 1997; Dominik 1998; Gaudi & Gould 1999; Dominik 2004b). A number of papers have reported on source properties (such as limb darkening) derived from the light curves of binary lens events (Albrow *et al.* 1999; Afonso *et al.* 2000; Albrow *et al.* 2000; Albrow *et al.* 2001a; Albrow *et al.* 2001b; Abe *et al.* 2003; Cassan *et al.* 2004).

Considerable theoretical work on the polarisation signatures from microlensing has also been carried out. Schneider & Weiss (1986) were the first to discuss the use of caustic crossings for inferring source intensity profiles. Schneider & Wagoner (1987) calculated the polarisation from the lensing of thick scattering photospheres of supernovae during such crossings. Simmons et al. (1995a,b) examined the polarisation from an electron scattering atmosphere being microlensed by a point mass, thus allowing the limb polarisation to be measured. Newsam et al. (1998) used this analysis to demonstrate that even relatively 'poor' polarimetric data can considerably improve the determination of stellar radii. In turn, Agol (1996) modelled the polarisation from an electron scattering stellar atmosphere by a binary lens. More recently, Simmons et al. (2002) examined the polarisation from an extended envelope for a point mass lens. The work of this paper applies the same atmosphere model as in Simmons et al. (2002) to the case of caustic crossings – arguably the 'best case scenario' for probing the extended envelope.

The structure of this paper is as follows. In Section 2 we discuss the microlensing of extended sources. In Section 3 we describe the polarisation intensity maps used in the calculation of the microlensing lightcurves. In Section 4 we provide representative lightcurves for both the polarisation and flux signals for a range of source parameters. We also discuss the observational implications of our results. The duration of caustic crossing events typically occurs over one night, so we believe that it is important to explore different observing strategies to find the most suitable way of observing these events while effectively recovering the source and envelope properties relative to the Einstein radius. Concluding remarks are presented in Section 5.

2 MICROLENSING OF EXTENDED SOURCES

The magnification of a point source by a point lens is given by

$$A_{\rm pt} = \frac{u^2+2}{u\sqrt{u^2+4}} \tag{1}$$

where u is the angular separation between the lens and source as normalized by the angular Einstein radius $\theta_{\rm E}$, which is given by

$$\theta_{\rm E} = \sqrt{\frac{4GM_{\rm L}}{c^2}\frac{(D_{\rm S}-D_{\rm L})}{D_{\rm L}D_{\rm S}}}, \tag{2}$$

where $M_{\rm L}$, $D_{\rm S}$, and $D_{\rm L}$ are the lens mass, the distance to source and the distance to lens respectively. The lensing is a transient event with $u = u(t)$ a function of time given by

$$u(t) = \sqrt{u_0^2 + \frac{(t-t_0)^2}{t_{\rm E}^2}}, \tag{3}$$

where t_0 is the time of maximum magnification at u_0 the impact parameter. The parameter $t_{\rm E}$ is the crossing time of $\theta_{\rm E}$:

$$t_{\rm E} = \theta_{\rm E}/\mu_{\rm rel}, \tag{4}$$

where $\mu_{\rm rel}$ is the relative proper motion between the lens and the source.

The point source approximation is valid when $\theta_{\rm S} \ll \theta_{\rm E}$, for $\theta_{\rm S}$ the angular radius of the source (which we shall assume is circularly symmetric). When this no longer holds – such as when the lens transits the source – the magnification is determined by an intensity-weighted integral over the projected surface of the source. The resultant is,

$$A_{\rm net}(t) = \frac{\int_0^{2\pi}\int_0^{\theta_{\rm S}} I(\theta,\alpha)A_{\rm pt}(u(\theta_L,\theta,\alpha,t))\,\theta\,d\theta\,d\alpha}{\int_0^{2\pi}\int_0^{\theta_{\rm S}} I(\theta,\alpha)\theta\,d\theta\,d\alpha} \tag{5}$$

where θ is an angular radius measured from the source origin, and α is an azimuthal angle about that origin. The angle $\theta_{\rm L}$ is the angular separation between the point lens and the source centre. The integral means that different emitting elements of the projected source make weighted contributions to the microlensing light curve according to their relative projected proximity to the lensing mass. Since this proximity is a function of time, an analysis of the event light curve allows for the possibility of determining the surface brightness profile of the source.

The magnification due to a binary lens system depends on additional parameters relating to the binary system: the mass ratio, the separation of the lenses, and the angle defining the trajectory of the source relative to the binary lens orientation. The magnification due to a binary lens has no simple analytic dependence on these parameters. However, near the fold caustic, the magnification can be approximated by

$$A_{\rm cau} = A_0 + \frac{b_0}{\sqrt{d}}, \tag{6}$$

where $d = d(t)$ is the angular distance (normalized to $\theta_{\rm E}$) from the caustic to a source element for all such elements interior to the caustic, A_0 is the constant magnification of the three non-caustic images, and b_0 is a scale factor related to specifics of the lens geometry and the ratio of $\theta_{\rm S}$ to $\theta_{\rm E}$ (e.g., the discussion of Castro *et al.* 2001). The literature of reports on caustic crossings by stars indicate typical observed peak magnifications of around 20–30 are common (e.g., Abe *et al.* 2003; Afonso *et al.* 2000; Albrow *et al.* 1999; Albrow *et al.* 2000; Albrow *et al.* 2001a; Albrow *et al.* 2001b). The sources are generally red giant stars, with radii of around $R_* \approx 10R_\odot$. With $\theta_{\rm S}/\theta_{\rm E} \sim 10^2$, values of b_0 are around 10, and values of A_0 are of order 3–10, as evidenced by the 'troughs' between successive caustic crossings (e.g., Alcock *et al.* 2000). The particular form of the approximation in Eq. 6 assumes that the caustic is a straight line (i.e., the source must be small compared to the curvature of the caustic) and that the caustic

crossing point is not in the vicinity of a cusp, where the magnification function takes a different form. Exterior to the caustic (yet near it so that the curvature of the caustic can still be ignored), the magnification will be constant with $A_{\rm cau} = A_0$. Note that the time-dependent variation of the polarised flux results entirely from the second term of Eq. 6 for intrinsically symmetric and unresolved sources.

3 POLARIZATION MODEL

We review now the intensity profile that will be used with Eq. 5 to calculate the microlensing lightcurves. As stated above the formalism follows that of Simmons et al. (2002). As emphasized in that work the model employed is well-suited to evolved cool stars. This class of stars exhibits stellar winds that are significantly stronger than the Sun's, with mass-loss rates ranging from $10^{-10} M_\odot$ yr^{-1} for typical red giants up to $10^{-5} M_\odot$ yr^{-1} for red supergiant and asymptotic giant branch stars (e.g., Lamers & Cassinelli 1999). The more extreme stellar winds are clearly dust-driven (e.g., Netzer & Elitzur 1993; Habing, Tignon, & Tielens 1994). Stars with milder winds are less understood, possibly driven by a combination of a Parker-style wind augmented by molecular and dust opacities (Jorgensen & Johnson 1992).

Assuming the flows are spherically symmetric, the run of the bulk gas density ρ in the wind with radius r will be given by

$$\rho = \frac{\dot{M}}{4\pi r^2\, v(r)}, \tag{7}$$

where $\dot{M}$ is the mass-loss rate, and $v(r)$ is the radial velocity of the flow, beginning subsonically and asymptoting to a terminal speed v_∞ at large radius.

The scattering opacity responsible for producing polarisation could be molecular Rayleigh scattering or dust scattering. Consequently, the density profile of the polarigenic species can differ from Eq. 7 by virtue of how molecules or dust are produced and destroyed as a function of radius. Particularly in the case of dust, the location of the condensation radius will be important. This latter point concerning dust is interesting, since the stars under consideration have photospheric effective temperatures of 3000–4000 K, whereas the dust condensation temperature is typically around 1500 K (Gail & Sedlmayr 1986). The implication is that dust-driven winds can have central cavities (not vacuums, but rather interior zones for which there is no significant scattering opacity). Models for dust-driven winds naturally predict the radial extent of these cavities, yet the condensation radius is largely unconstrained by observations (Bloemhof & Danen 1995). Microlensing can provide relevant observational constraints on the location of the condensation radius. For this pilot study of the polarimetric signals from caustic crossing events, we choose to parametrize the scattering number density by a simple power-law with

$$n(r) = n_0 \left(\frac{R_*}{r}\right)^\beta, \tag{8}$$

instead of fretting about the details of the wind acceleration, or how the scattering opacity evolves in the flow. We additionally assume the envelope is optically thin for this application, but will explore optical depth effects of the envelope in a subsequent paper.

We adopt the Stokes vector notation $\mathbf{I} = (I, Q, U, V)^T$ for the intensities, and $\mathbf{F} = (F_I, F_Q, F_U, F_V)^T$ for the fluxes. Following the notation of Simmons *et al.* (2002), the Stokes intensities for direct and scattered light will be given by

$$\begin{aligned}\mathbf{I}(p,\alpha) &= \mathbf{I_0}(p) + \frac{3}{16} I_* (\beta - 1) \left(\frac{R_{\rm h}}{p}\right)^{\beta-1} \left(\frac{R_*}{p}\right)^2 \\ &\quad \times \tau_{\rm sc}\, g_0(p) \begin{pmatrix} G_{\rm I} \\ G_{\rm P}\cos(2\alpha) \\ -G_{\rm P}\sin(2\alpha) \\ 0 \end{pmatrix}\end{aligned} \tag{9}$$

where $R_{\rm h}$ is the radius for any 'hole' of scattering opacity, and the total optical depth, $\tau_{\rm sc}$ is defined as

$$\tau_{\rm sc} = \frac{n_0 \sigma R_{\rm h}}{\beta - 1}, \tag{10}$$

with σ the scattering cross section, and where the scatterers are taken to exist only for $r \geqslant R_{\rm h}$.

For simplicity we shall assume a uniform surface brightness profile for the star, such that

$$\mathbf{I_0}(p) = \begin{cases} (I_*, 0, 0, 0) & \text{for } p < R_* \\ 0 & \text{for } p \geqslant R_* \end{cases} \tag{11}$$

where I_* is the intensity of the star. Although we ignore limb darkening, its main effect would be to enhance the polarisation from lines-of-sight that are close to the star (bearing in mind that we are currently ignoring scattering polarisation from the stellar photosphere, an assumption that we shall justify *a posteriori*). The reason is that at a fixed distance from the star, limb darkening causes the stellar radiation field impinging upon a given point at this distance to be more radially directed than is the case for a uniformly bright star (Cassinelli, Nordsieck, & Murison 1987).

Also appearing in Eq. 10 is the stellar occultation factor, g_0, that is given by

$$g_0(p) = \begin{cases} 1/2 & \text{for } p < R_*, \\ 1 & \text{for } p \geqslant R_*. \end{cases} \tag{12}$$

The occultation factor simply accounts for the fact that radiation scattered on the far side of the star will not reach the observer. The integral factors $G_{\rm I}$ and $G_{\rm P}$ are

$$\begin{aligned} G_{\rm I} &= \int_0^{s_{\rm max}} \sqrt{s^{\beta+1}} \sqrt{\frac{1-sq}{1-s}} \\ &\quad \left\{ \frac{8}{3} \left(\frac{1}{s^2 q}\right) \left[(1-sq)^{-1/2} - (1 - \frac{1}{4} sq) \right] - 1 \right\} {\rm d}s \end{aligned} \tag{13}$$

and

$$G_{\rm P} = \int_0^{s_{\rm max}} \sqrt{s^{\beta+1}} \sqrt{\frac{1-sq}{1-s}} ds \tag{14}$$

with $s = (p/r)^2$, $q = (R_*/p)^2$, $s_{\rm max} = (p/r_{\rm min})^2$, for

$$r_{\rm min} = \max(R_{\rm h}, p), \tag{15}$$

where z is the line-of-sight coordinate and $r^2 = p^2 + z^2$.

The fluxes during the microlensing event are then computed from the integral expressions:

$$F_{\rm I} = \int_0^\infty \int_0^{2\pi} I(p,\alpha)\, A_{\rm cau}(d)\, p\, dp\, d\alpha, \tag{16}$$

$$F_{\rm Q} = \int_0^\infty \int_0^{2\pi} I(p,\alpha)\, \cos 2\alpha\, A_{\rm cau}(d)\, p\, dp\, d\alpha, \tag{17}$$

$$F_{\rm U} = \int_0^\infty \int_0^{2\pi} I(p,\alpha)\, \sin 2\alpha\, A_{\rm cau}(d)\, p\, dp\, d\alpha, \tag{18}$$

$$F_{\rm V} = 0. \tag{19}$$

As is usual, the observed fractional polarisation can then be calculated as

$$P = \frac{\sqrt{F_{\rm Q}^2 + F_{\rm U}^2 + F_V^2}}{F_{\rm I}} \tag{20}$$

where the total flux $F_{\rm I}$ is a sum of the direct stellar flux F_* and the scattered intensity $F_{I_{\rm sc}}$. The polarisation position angle is defined as

$$\psi = \frac{1}{2} \tan^{-1} \frac{F_{\rm U}}{F_{\rm Q}}. \tag{21}$$

4 RESULTS

Having described the lensing approximation for a straight fold caustic, and the underlying source model, we have conducted a parameter study for microlensing light curves associated with caustic crossing events as various source and lens properties are varied. In displaying results, our goal is to highlight those features that pertain to elucidating the properties of the source; therefore, instead of light curves as a function of time, we choose to plot flux observables as a function of caustic position relative to the star. To do so, we define the coordinate $x_{\rm lens}$ as the normal projected distance between the straight line caustic and star centre in the source plane. Then $y_{\rm lens}$ is the coordinate along the caustic direction. Both coordinates are normalized to the stellar radius R_*. The case $x_{\rm lens} < 0$ is when the star centre lies inside the caustic; the case $x_{\rm lens} > 0$ is when the star centre lies outside the caustic; and $x_{\rm lens} = 0$ is the moment of transit for the star centre.

Conversion to a time coordinate is achieved with $t = (x_{\rm lens}\, R_*)/(D_{\rm S}\, \mu_{\rm rel,x})$, where $\mu_{\rm rel,x} = \mu_{\rm rel} \cos\gamma$, with $\mu_{\rm rel}$ the magnitude of the relative proper motion between the source and caustic, and γ is the trajectory orientation of the source relative to the caustic. So $\gamma = 0^\circ$ means the source is traveling in the $+x$ direction in the frame of the caustic, whereas $\gamma = \pm 90^\circ$ means the source is moving in the $\pm y$ direction, respectively. The orientation of the trajectory has no bearing on the shape of the lensing light curves in time, except as a 'stretch' factor for scaling purposes; for example, γ does not affect the value of the peak polarisation achieved during the event.

4.1 Test Case

Figure 1 shows model results for a test scenario. The upper panel shows the flux of the source, relative to the case of being unlensed, as a function of the caustic location. The lower panel is for the polarised flux, also normalized to the unlensed flux of the source F_0, and multiplied by 100 to simulate a kind of percent polarised flux (the reason for this rather odd choice will become apparent in a moment). The envelope parameters are fixed with an envelope optical depth of $\tau_{\rm sc} = 0.1$, density parameter $\beta = 2$, and no cavity (i.e., $R_{\rm h} = R_*$). The lens parameter b_0 is fixed at a value of 10, but A_0 is allowed to vary from 1 to 15, with larger values giving stronger peak flux magnifications.

We have argued that A_0 should have no bearing on the polarised emission, and indeed that is seen to be the case in Figure 1. All of the variation of the polarized flux comes from the second term in Eq. 6 with scaling b_0. In the standard representation of polarisation with $p = F_{\rm Q}/F_{\rm I}$. The fractional or percent polarisation can be affected by the value A_0, because the total flux variation as the microlensing event evolves does depend on A_0. A value of $A_0 = 1$ has been adopted for the rest of the model calculations.

It is useful at this point to introduce a schematic figure that demarcates regions contributing to the polarised light as the caustic crossing evolves. Figure 2 shows four panels, with the source moving from inside the caustic to outside in the sequence (A) to (D). The vertical dotted line is the caustic, hence the left region is interior to the caustic and the right region is outside it. The star is the cross-hatched region. The double-headed arrows show the sense of orientation that would result for the emergent polarised flux from right angle scattering in the plane of the sky if the source were resolved. The dashed diagonal lines are where $Q = 0$. Thus the figure is useful in mapping how the different zones of polarised flux will contribute to the total polarised emission from the unresolved lensed source as a function of its location relative to the caustic line.

The variation of the model polarised flux shows interesting sign changes. Here we are assuming an observational scenario in which a second exiting caustic crossing has been predicted from an earlier interior crossing event. Thus in Figure 2 at time (A), the source is approaching the caustic to exit. The quadrant closest to the fold is dominated by scattered light with $Q > 0$, and so initially the polarisation is oriented parallel to the fold caustic in the sky. As the event progresses, the situation of case (B) is reached. Only scattered light leftward of the caustic will be subject to a magnification *gradient*, thus breaking the symmetry and leading to a net observed polarisation. By time (B), the light being most strongly magnified is for $Q < 0$, and so the polarisation position angle has rotated 90° by the time the caustic is first tangent to the photosphere. By time (C), a minimum in the polarised flux has passed. Now the polarisation changes rapidly, so that by the time the caustic is tangent to the far side of the photosphere, the polarised flux has changed sign again, becoming positive. Note in terms of the polarised light $F_{\rm Q}/F_{\rm I}$, the percent polarisation will rise significantly, because the magnification of the stellar photosphere is minimized once the photosphere has completely exited the caustic.

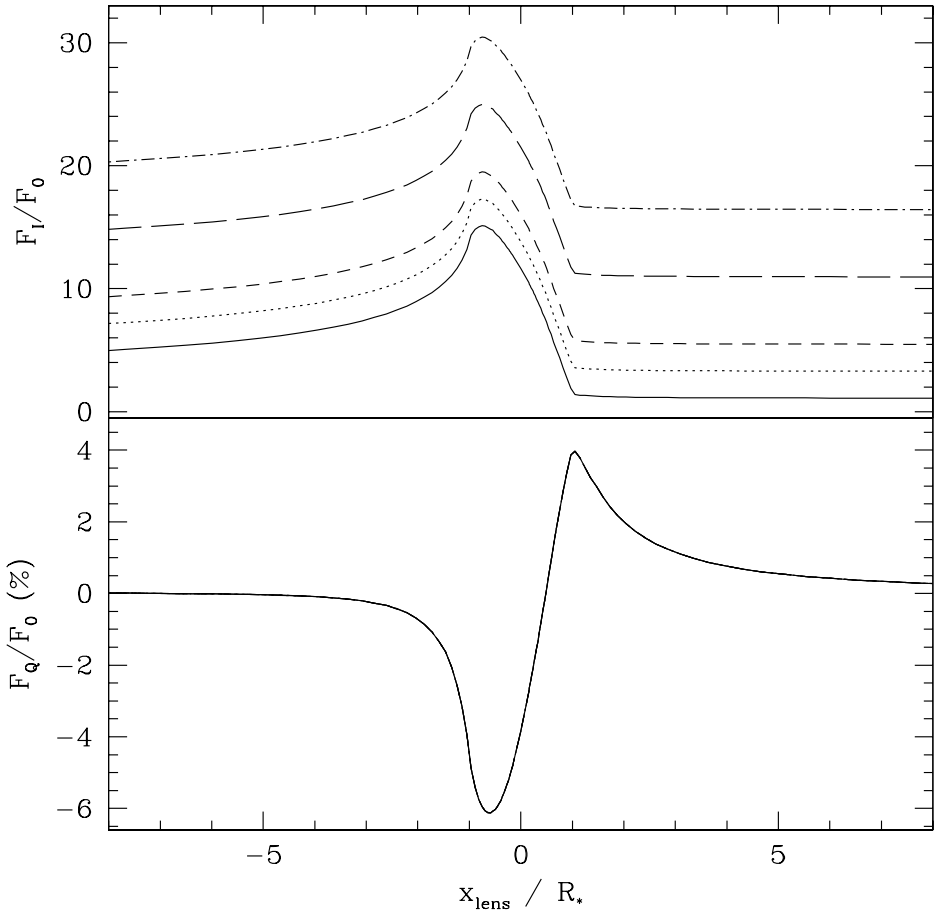

Figure 1. Plots of the variation in total flux (upper panel) and the normalized polarised flux (lower panel) for a scattering envelope during a fold caustic crossing event. The lower axis displays the location of the caustic in the source plane (normalized to R_*) with respect to the centre of the star, with negative values for when the star lies *interior* to the caustic, and positive values for when it lies *exterior*. Values of $\beta = 2$, $R_{\rm h} = R_*$ (no cavity), and an envelope optical depth of $\tau_{\rm sc} = 0.1$ are adopted. A lens parameter of $b_0 = 10$ is fixed, but A_0 takes values of $1, 3, 5, 10$, and 15 (in order of increasingly stronger peak fluxes). As described in the text, variations in A_0 change the total flux light curves, but not the polarisation, because A_0 is a constant of the integration on either side of the fold caustic. It is b_0 and the properties of the envelope that set the shape and amplitude of the polarimetric variations.

4.2 Variable Envelope Optical Depth

Figure 3 shows the response of the flux and polarisation light curves to different values of envelope optical depth. The lower panel now plots the standard form of polarisation, $p = F_{\rm Q}/F_{\rm I}$, and hereafter. Values of $\tau_{\rm sc} = 0.001, 0.01, 0.1, 0.3$, and 1.0 are used. A value of $A_0 = 1$ and $b_0 = 10$ are used with a density distribution described by $\beta = 2$. These values for A_0, b_0, and β will be standard in our calculations unless noted otherwise. The envelope has little effect on the flux light curve except when $\tau_{\rm sc} \gtrsim 0.1$. On the other hand, the amplitude of the polarisation light curve is approximately linear in $\tau_{\rm sc}$.

The envelope is reasonably thin, and so the flux magnification is dominated by the photospheric emission. Agol (1996) has investigated the polarimetric variations from scattering polarisation in stellar atmospheres. We have purposely ignored photospheric contributions to the polarised emission, because circumstellar envelopes are more efficient at producing polarised emission (albeit, this is a function of optical depth), and because we wish to investigate the effects of a circumstellar envelope for the light curves. Although A_0 and b_0 are not exactly the same, the case of the solid line in the upper panel of Figure 3 is roughly comparable to the $r = 0.01$ case shown in the upper panel of Agol's Figure 1.

Overall, the polarisation curves are generally similar to those of Agol (1996); however, there are notable quantitative and qualitative differences. First quantitatively, the peak polarisation achieved by photosphere crossings were rarely in excess of 1%, and in some cases only a few tenths of a percent, whereas thin scattering envelopes can achieve values in excess of 5% when $\tau_{\rm sc}$ is large enough ($\tau_{\rm sc} \gtrsim 0.5$).

There are qualitative differences as well. The underlying source models are drastically different. For example, a stellar

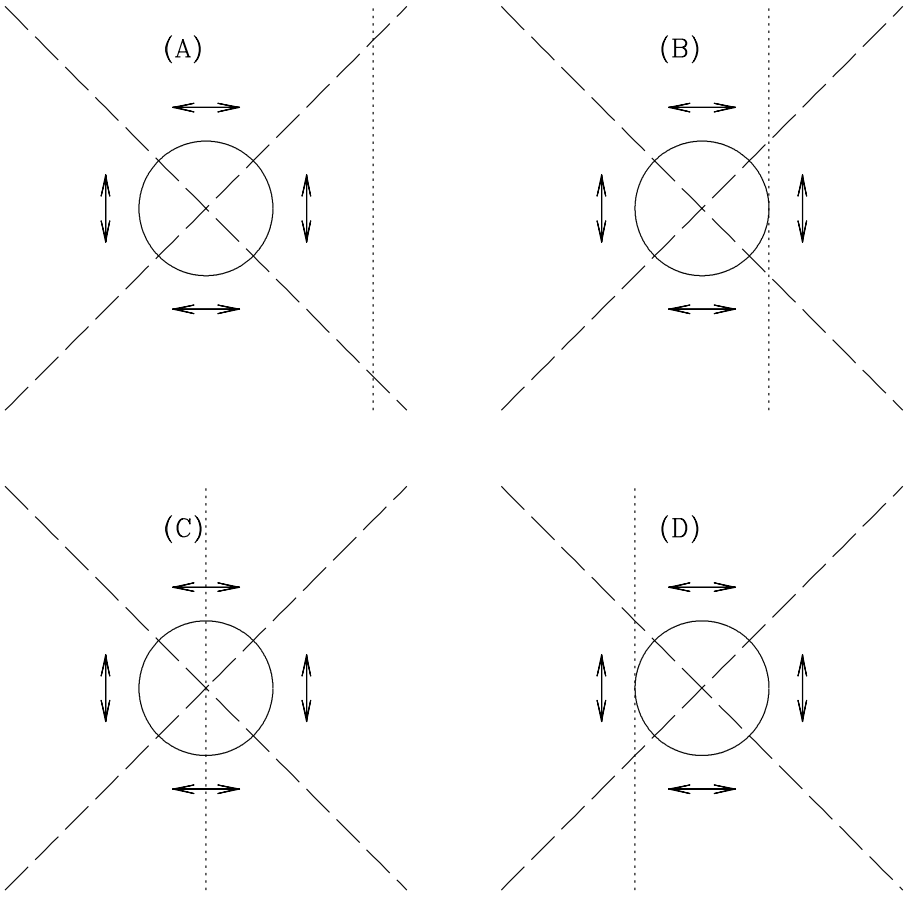

Figure 2. Schematic of the geometry for the transit of the star and circumstellar envelope across a fold caustic. Shown are four times (A) – (D). The star is cross-hatched. The vertical dotted line is the caustic, with left being interior and right being exterior. The double-headed arrows are representative polarisation vectors at those points (vertical being $Q > 0$ and horizontal being $Q < 0$). Finally, the diagonal dashed lines are the locus of points where the emergent Q-intensity would be zero; these then are 'null' lines where Q switches sign, and the polarisation position angle rotates 90° between adjacent zones.

photosphere has an intrinsic polarisation profile (as a function of p) that is maximum at the stellar limb and decreases to zero at the centre of the star. In our case the photospheric polarisation is ignored because it is small compared to the envelope polarisation. The extended envelope has a polarisation profile that is zero at large distance from the star, and increases toward the stellar limb. The polarisation peaks outside the stellar limb, and decreases to zero again at the stellar centre. So the source models are quite different, but at the same time the variable polarisation from microlensing for the two cases are somewhat similar. Basically, the photospheric polarisation has a discontinuous jump in moving from off the star across the stellar limb, whereas the circumstellar envelope has a more gradual peak off the stellar limb. Microlensing involves a weighted surface integral, thus 'smoothing' over these detailed differences, leading to somewhat similar light curves (Dominik 2004a). Still, the fact that the peak polarisation appears at the stellar limb for a photosphere in a discontinuous way explains why there is a peak (sometimes cuspy) at $x_{\rm lens} = -R_*$ in Agol's models and not in ours. (This is $y_* = -r$ in Agol's notation; see his Fig. 1.)

4.3 The Influence of a Cavity

Figure 4 shows how a cavity of scatterers at the inner envelope impacts the polarisation light curves. The different curves are for different 'hole' radii of $R_{\rm h} = 1.0, 1.5, 3.0, 5.0$ and $8.0 R_*$. Clearly, as the extent of the cavity increases, the polarimetric variation occurs over a longer time-scale, with the peak polarisation shifting toward larger values of positive $x_{\rm lens}$, and the negative 'trough' growing in extent toward negative $x_{\rm lens}$ as a precursor to the transit of the star.

In each case the envelope optical depth is maintained at $\tau_{\rm sc} = 0.1$. First, this is rather optically thin, as evidenced by the total flux light curve (upper panel) which does not vary much between the different cases, and is dominated largely by

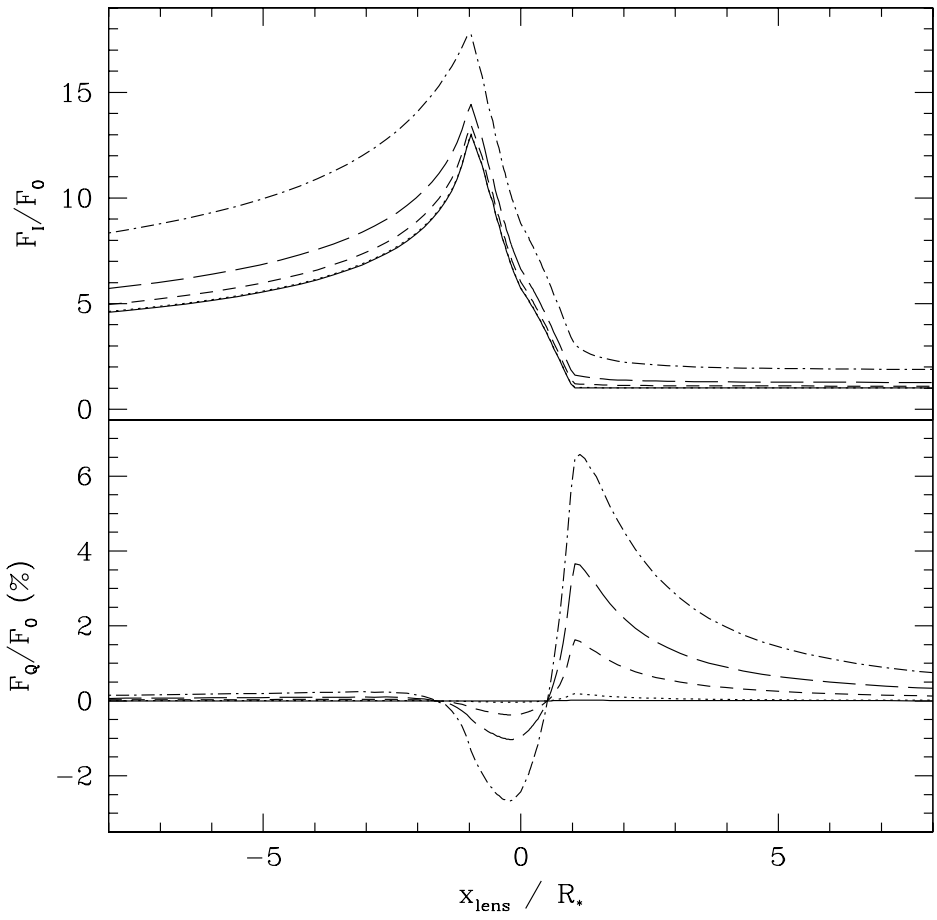

Figure 3. Plots like Fig. 1, but now with fixed lens parameters and variable envelope optical depths, and with the lower panel as percent polarisation (normalized by the total intensity flux $F_{\rm I}$). In this case values of $\beta = 2$, $R_{\rm h} = R_*$ (no cavity), $A_0 = 1$, $b_0 = 10$ are assumed. The different curves are for different envelope scattering optical depths, with $\tau_{\rm sc} = 0.001, 0.01, 0.1, 0.3$, and 1.0 (in order of increasingly stronger peak polarisations). Note the change in sign of the polarisation as the stellar photosphere transits the caustic, and the strong peak value that results immediately after the photosphere has completely exited the caustic.

the photosphere. Second, the scale of the polarisation is to zeroth order determined by the value of $\tau_{\rm sc}$, which explains why all of the curves have similar peak polarisation values. Third, holding $\tau_{\rm sc}$ constant implies conserving the total number of scatterers; hence although the different cases shown have the same density distribution at $\beta = 2$, these require different density scales n_0, so as to maintain fixed $\tau_{\rm sc}$. Using Eq. (10), the density scale for fixed envelope optical depth is given by

$$n_0 = (\beta - 1)\,\frac{\tau_{\rm sc}}{\sigma\, R_{\rm h}} \tag{22}$$

So our approach for inserting a cavity is not to delete scatterers, but to redistribute them outward. The goal of considering cavities is to illustrate how microlensing can neatly trace the cavity extent through the polarisation light curve, which is relevant for the case of red giants that can form dust in their winds at a condensation radius that is offset from the stellar photosphere.

Figure 5 shows the same curves of Figure 4, but with $x_{\rm lens}$ normalized to $R_{\rm h}$ instead of R_*, which nicely shows how the polarimetric variations are set by the crossing of the cavity. Clearly, the peak polarisation is affected by the cavity (generally smaller), and substructure is seen around the passage of the photosphere from inside the caustic to outside. The peak polarisation consistently occurs just before the cavity transits entirely out of the caustic, and so becomes an excellent tracer of the cavity extent relative to the stellar radius, which can be determined from the total flux variations.

In other words the total flux variations show a peak at a time when the stellar limb just begins to transit the caustic. As the event proceeds, the total flux shows a precipitous drop, and then goes flat. The extended envelope can produce a tail of enhanced brightness after the star has transited out of the caustic, but the drop is dominated by the star. So that time-scale is $2t_* = 2\theta_*/\mu_{\rm rel}$, where θ_* is the angular radius of the star. On the other hand, from this time until the peak polarisation

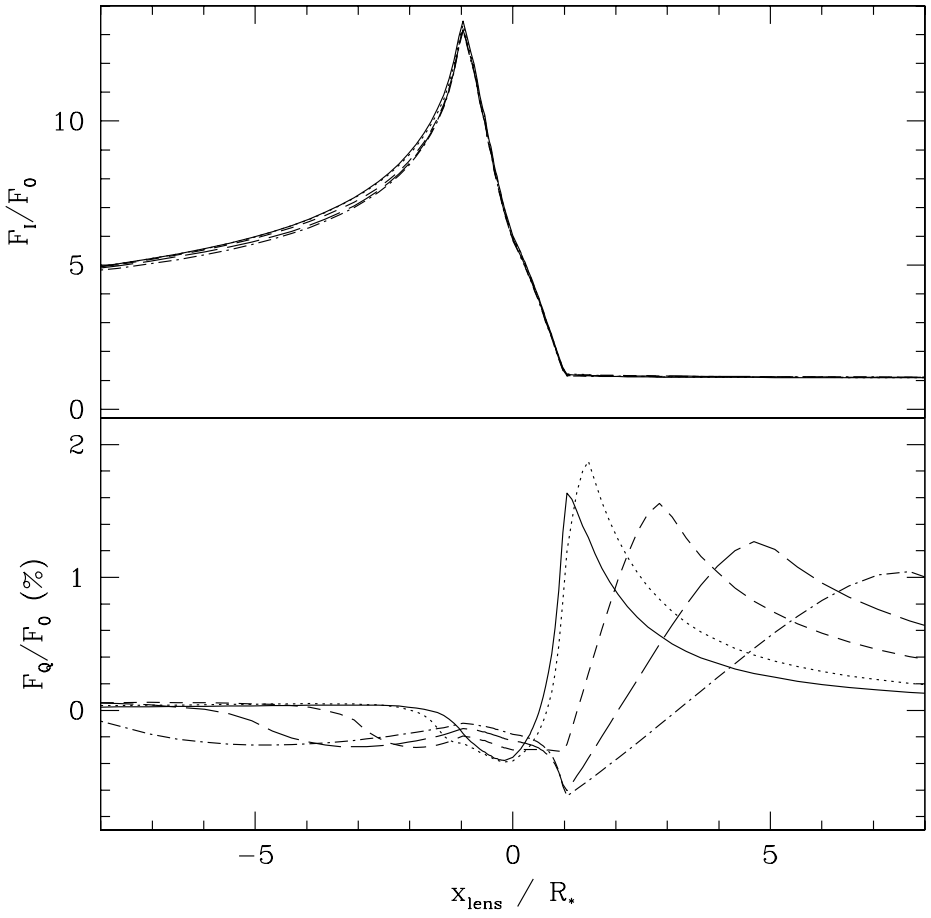

Figure 4. Illustration of how a cavity of scattering opacity impacts the polarisation variation. All of the curves are for $\tau_{\rm sc} = 0.1$. Each is distinguished by the extent of the cavity, with $R_{\rm h} = 1.0, 1.5, 3.0, 5.0$, and $8.0R_*$, with larger cavities yielding peak polarisations at larger values of $x_{\rm lens}$. Note that the total flux curve (upper panel) is little influenced by the cavity extent because the scattering envelope is optically thin. Although basically similar, there are some notable qualitative differences in the variation of polarisation when a cavity is present (see Fig. 5).

is achieved will require a time $t_{\rm h} = \theta_{\rm h}/\mu_{\rm rel}$. Consequently $R_{\rm h}/R_*$ will be given by $t_{\rm h}/t_*$.

4.4 The Impact of the Density Distribution

Models for the flux and polarisation variations have been generated for different envelope density distributions, and the results are displayed in Figure 6. The curves are for $\beta = 1.5, 2.0, 2.5, 3.0$ and 4.0. A cavity with $R_{\rm h} = 3.0R_*$ has been adopted.

The different cases are all for a fixed value of $\tau_{\rm sc} = 0.1$. As noted before, this is in essence achieved via redistribution of scatterers. In this case there is a fixed hole. Changing β makes the density distribution more or less steep. As β is made to increase, keeping $\tau_{\rm sc}$ fixed results in increased values of n_0, and so the peak polarisation that is dominated by the number density of scatterers at the limb of the cavity increases as well.

So β does not necessarily lead to larger polarisations; here it is an artefact of maintaining a constant value of $\tau_{\rm sc}$. Fundamentally what β does is to alter the slope of the polarisation curves after the cavity has completely passed out of the caustic, making the slopes steeper with increasing β. In fact, in the limit that the star can be treated as a point source, the asymptotic slope of the polarisation for relatively large values of $x_{\rm lens}$ can be derived analytically. The derivation is found in the Appendix; here just the result is quoted. Asymptotically, the polarised flux (*not* the percent polarisation) will be given by

$$F_{\rm Q} \propto \left(\frac{R_{\rm h}}{x_{\rm lens}}\right)^{(2\beta-1)/2} \propto t^{-(2\beta-1)/2}. \qquad (23)$$

So larger values of β lead to steeper declines in the polarised flux as the microlensing event progresses. Two points should be mentioned. First, although real sources may not follow a power-law distribution for the density of scatterers in portions of their extended envelopes, a value of $\beta = 2$ is reasonable to expect at large scale for a spherical wind flow, for which case $F_{\rm Q} \propto t^{-3/2}$. Second, the preceding equation is only

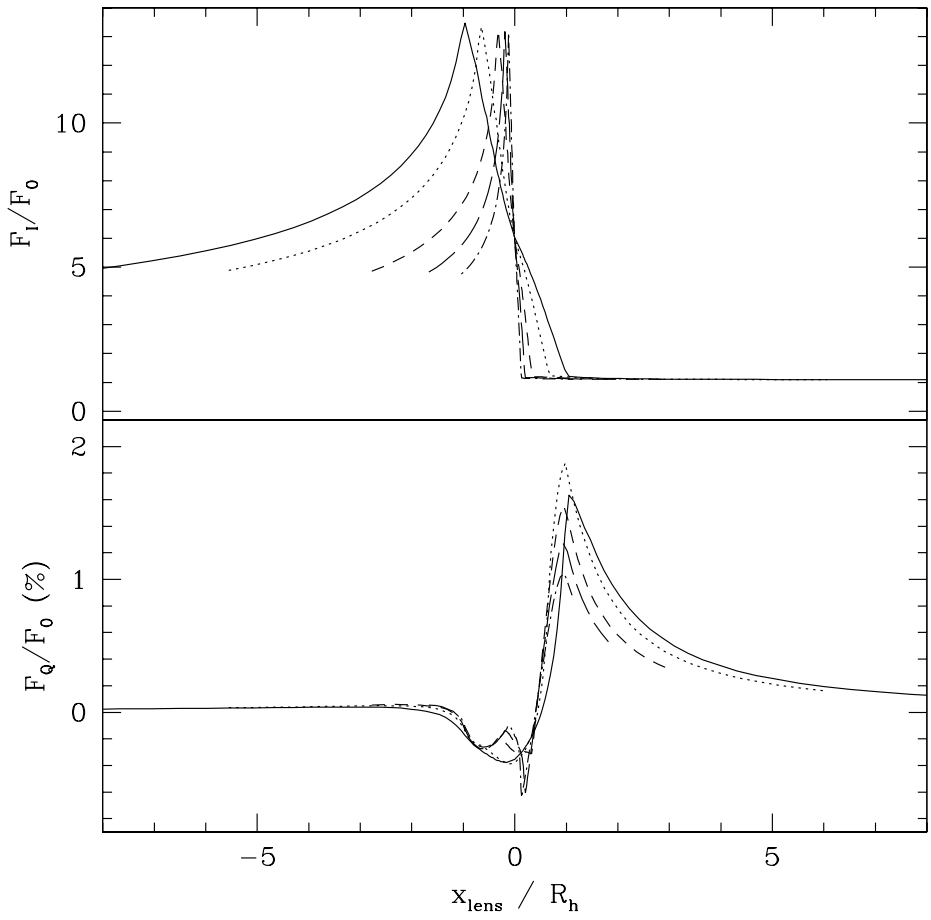

Figure 5. The results shown in Fig. 4, except now the lower axis for the position of the fold caustic is normalized to the size of the cavity $R_{\rm h}$. From Fig. 4, the total flux variation was set by the passage of the photosphere across the caustic. The polarimetric variations on the other hand are determined the size of the cavity. Although the positive peak polarisation has variable width, the negative 'trough' has approximately constant width. The solid line is for no cavity (i.e., $R_{\rm h} = R_*$); notably the presence of a cavity changes the qualitative shape of the trough, with some recovery toward net zero polarisation followed by a sharp drop toward more negative values.

valid both for when the star can be treated as a nearly point source of illumination with respect to the scattering envelope and when the caustic can be approximated as a straight line. Even if the asymptotic trend of Eq. (23) is not achieved in a real event, it does provide useful insight and limiting behavior for the modeling effort.

4.5 Variation of the Magnification Gradient

Figure 7 shows model results as the value of b_0 is varied, with values of $3, 5, 8, 12$, and 17 (with $A_0 = 1$ fixed). With b_0 relatively large compared with A_0, the polarisation varies little for $x_{\rm lens} < 1$, prior to when the star has passed out of caustic. The reason is that the polarisation is a ratio of the polarised light to the total flux, and both scale as b_0. Clearly, the total flux shown in the upper panel is strongly dependent on b_0, increasing essentially linearly with b_0. Similarly, the polarisation *after* the star has passed out of the caustic is affected by b_0, because now $F_{\rm I}$ is a constant that depends primarily on the photospheric flux multiplied by A_0, whereas $F_{\rm Q}$ still depends on the value of b_0.

5 DISCUSSION

This study has demonstrated that polarimetric observations of caustic crossing events could be used to probe circumstellar envelopes. Such data could constrain the number density of the scatterers within the envelope, detect the presence and trace the extent of a central cavity around the source photosphere, and provide information about the density distribution of scatterers.

To summarize, a comparison of the time-scale for the total flux variations against that of the polarimetric variations yields the extent of the cavity relative to the stellar radius. In the case of dust producing cool star winds, that informa-

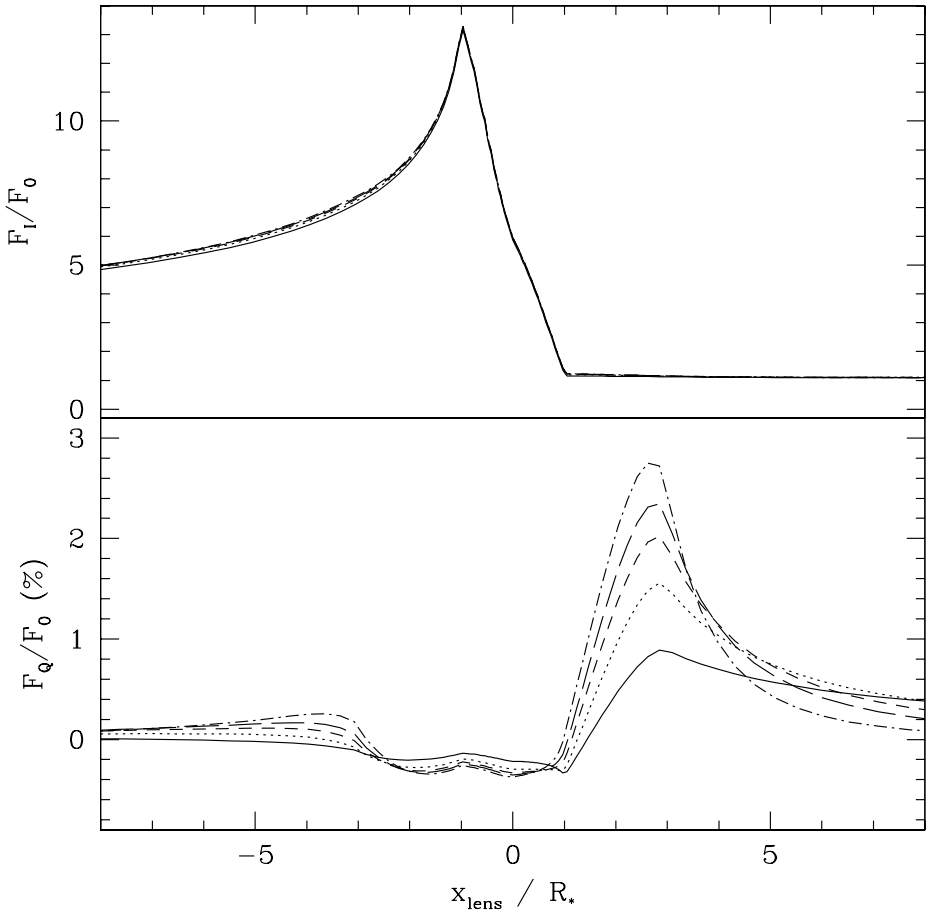

Figure 6. Here only the value of β is allowed to vary. The flux light curve hardly changes, whereas the polarimetric profiles, although similar qualitatively, are seen to vary significantly in amplitude. The values of β are 1.5, 2.0, 2.5, 3.0, and 4.0, in order of stronger positive peak polarisations, and the envelope sports a cavity with $R_{\rm h} = 3.0R_*$.

tion is sufficient to test models that predict the location of the dust condensation radius. The late time evolution of the polarised flux is set by the density distribution (our β-value for this work). Lens parameters A_0 and b_0 can be derived from fitting the variation of the photospheric flux during the caustic crossing, in which case model fits to the polarisation level will give the value of $\tau_{\rm sc}$ for the circumstellar envelope.

To connect our model results with applications to observed events, we must relate the envelope properties for the model to those of real sources. Some help toward this end is provided by Netzer & Elitzur (1993), who describe model results for dust-driven winds. In their Eq. (10), they provide an expression relating stellar parameters $\dot{M}$, v_∞, and L_* to the flux mean optical depth of the envelope $\tau_{\rm F}$:

$$\frac{\dot{M}}{2\times10^{-5}\,M_\odot\ {\rm yr}^{-1}} = \tau_{\rm F}\,\frac{L_*/10^4 L_\odot}{v_\infty/10\,{\rm km\ s}^{-1}}, \qquad (24)$$

here shown in slightly modified form from their paper. The value of $\tau_{\rm F}$ will not equal the value of $\tau_{\rm sc}$ that we use to characterize our models; however, the flux mean opacity does give an overall scale related to the optical depth of the envelope. Although relating $\tau_{\rm sc}$ to $\tau_{\rm F}$ will depend on the particular opacities involved, one might generally expect that the two will scale together. The models of Netzer & Elitzur show that the minimum mass-loss for dust driving to be dominant is around $10^{-7}\,M_\odot$ yr^{-1}. At this value for a star with $L_* = 10^4 L_\odot$ and $v_\infty = 10$ km s^{-1}, the flux mean optical depth will be 0.02 (of course, the optical depth at a wavelength of interest can be higher or smaller).

One of the challenges in detecting polarized signals in real events, such as this hypothetical Bulge star, is that the crossing of the caustic by the photosphere will typically take only a few hours (e.g., Alcock *et al.* 2000). We can estimate the detectability of polarizations predicted by our models. Using a Kurucz model for a cool subgiant of $g = 3.5$ and $T = 4500$ K (parameters similar to OGLE-1999-BUL-23 from Albrow *et al.* 2001), the I-band flux at a distance of 8 kpc is estimated to be 3×10^{-13} erg s^{-1} cm^{-2}, with a corresponding magnitude of about $m_I \approx 18$. Of course, during the lensing event, the source brightens, and magnifications by

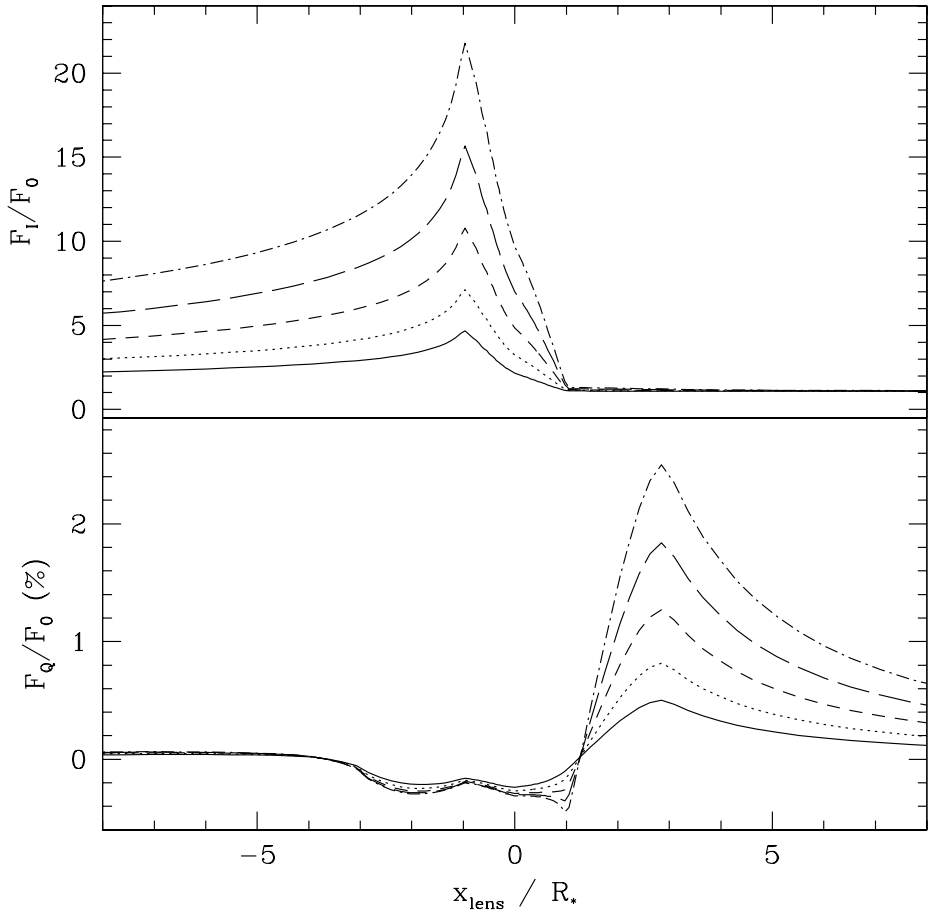

Figure 7. These figures are for fixed envelope properties, but for different values of the lens parameter $b_0 = 3, 5, 8, 12$, and 17 and A_0 fixed at unity. Both the strength of the peak flux and peak polarisation vary almost linearly with the value of b_0. Variations in A_0 would have no effect on the polarisation, but would influence the total flux curves.

an order of magnitude are typically achieved, at which point $m_I \approx 15.5$. The time t required to achieve a given signal-to-noise ratio S/N for a telescope of diameter D in centimeters, allowing for Poisson noise only, will be

$$t \approx 9\frac{(S/N)^2}{D^2}. \tag{25}$$

Our models indicate that peak polarizations of about 1% will be achievable during caustic crossings. A 5σ detection at this polarization level requires $S/N = 500$. Additionally, exposures are needed at 8 position angles in order to construct the Stokes I, Q, and U fluxes (eight to eliminate systematics). Consequently, the required exposure time in total for this detection level, not counting overhead, will be a little over 30 minutes using a 1-meter telescope. Although this exposure estimate is a lower limit (owing to neglect of background, inefficiencies, and telescope overheads), the required exposure is about 10% of the duration of the photosphere crossing, even smaller for the bulk of the circumstellar scattering envelope, and can be reasonably obtained with modest facilities equipped with polarimetric instrumentation.

Although the original goal of microlensing surveys was to deduce the properties of dark matter in the Milky Way, it is clear that a vast range important of by-products have resulted from the survey effort, from catalogs of variable stars to observations of finite source effects (as described in the Introduction). Our contribution to the topic of finite source effects has been to point out how novel and valuable information about circumstellar envelopes might be obtained through polarimetric monitoring of events involving binary lenses and sources that may have substantial winds.

Certainly, our models include some simplifying assumptions, such as ignoring polarisation from the photosphere and the effect of limb darkening. Neither of these are severe; indeed, both will tend to *increase* the peak polarisations above those predicted by our models. Photospheric polarisation is expected to be smaller than the circumstellar contribution for stars with significant winds, but its contribution should add to the Q and U fluxes constructively, and not destructively.

Limb darkening will tend to mollify the effects of the finite depolarisation factor, thereby increasing the peak polarisation from the inner wind where the density of scatterers is larger (although limb darkening will have little or no impact in the case of significant central cavities). We have also not allowed for optical depth effects, by way of multiple scattering effects and extinction of the photospheric emission. We intend to consider these effects in a separate paper. However, substantial scattering optical depths will be more important for quite dense winds, like those of red supergiants and asymptotic giant branch stars. For the more common red giant stars, the optically thin assumption will be a good assumption.

ACKNOWLEDGEMENTS

The authors are grateful to an anonymous referee who made critical comments that led to needed clarifications of the text. This research was supported by a grant from the National Science Foundation (AST-0354262).

APPENDIX A: OBTAINING β FROM THE ASYMPTOTIC DECLINE OF THE STOKES Q-FLUX

Consider a source that lies inside the caustic and is passing out of it. (The arguments that follow also hold true when the source first approaches the caustic.) After the photosphere of the star has completely passed out of the caustic, the polarisation achieves a strong positive (by our convention) peak value. This occurs because only the scattering envelope lies interior to the caustic and so is subject to the selective amplification, whereas the photosphere is amplified by an approximately constant value. As the event evolves, more of the envelope transits the fold caustic, and the polarised signal at a given moment is given primarily by the highest value of the polarised flux along the caustic itself. The scale of this polarisation is set by the scattering optical depth of the envelope, but the slope of the polarised flux light curve is determined by the density distribution of scatterers. Here, we derive this relation between the lens position and the dependence of the polarisation on β.

As the star moves farther along from the caustic, the scattered light is accurately described by a point source. Equation (10) indicates that far from the star, $Q(p,\alpha) \approx Q_0\,(R_{\rm h}/p)^{\beta+1}\cos 2\alpha$. The polarised flux will be given by

$$\begin{aligned} F_{\rm Q} &= \frac{R_*^2}{D^2}\int_0^\infty dx\,A(x)\int_{-\infty}^{\infty} dy\,Q(p,\alpha) \\ &= Q_0\,\frac{R_*^2}{D^2}\int_0^\infty dx\,\frac{b}{\sqrt{x}}\int_{-\infty}^{\infty} dy\,\frac{(x+x_l)^2-y^2}{(x+x_l)^2+y^2} \\ &\quad\times\left[\frac{R_{\rm h}^2}{(x+x_l)^2+y^2}\right]^{(\beta+1)/2}. \end{aligned} \tag{A1}$$

Factoring out $(x+x_l)$ and making a suitable change of variable, the integration in y can be evaluated numerically for any particular value of β. For β an integer, analytic integration formulae will apply. Because the result is not critical for our concerns, we simply denote the result of the y integral as $Y(\beta)$, giving

$$F_{\rm Q} = Q_0\,b\,R_{\rm h}^{\beta+1}\,\frac{R_*^2}{D^2}\,Y(\beta)\int_0^\infty \frac{dx/\sqrt{x}}{(x+x_l)^\beta}. \tag{A2}$$

Using a substitution with $z=\sqrt{x/x_l}$, the integral will have a similar form as the one for y, but with a different dependence on β. We define the result of this integration to be $X(\beta)$, leading to

$$F_{\rm Q} = Q_0\,b_0\left(\frac{R_{\rm h}}{x_l}\right)^{(2\beta-1)/2} R_{\rm h}^{3/2}\,\frac{R_*^2}{D^2}\,X(\beta)\,Y(\beta). \tag{A3}$$

Observationally, the lens position is linear with time t, and so $\log F_{\rm Q} = -\frac{2\beta-1}{2}\log t + \log t_0$, where the other factors have been collected into the variable t_0. Of course this is a power-law, and its slope is directly related to the value of β for the density distribution of scatterers in the envelope. For example, many of our models employ $\beta=2$, in which case the asymptotic polarised flux varies as $F_{\rm Q}\propto t^{3/2}$. It should be pointed out that this limiting behavior will only be achieved in the tail of the polarised light curve, somewhat following the polarimetric peak.

REFERENCES

Abe, F., et al., 2003, A&A, 411, L493
Afonso, C., et al., 2000, ApJ, 532, 340
Agol, E., 1996, MNRAS, 279,571
Albrow, M., et al., 1999, ApJ, 522, 1011
Albrow, M., et al., 2000, ApJ, 534, 894
Albrow, M., et al., 2001a, ApJ, 549, 759
Albrow, M., et al., 2001b, ApJ, 550, L173
Alcock C., et al., 2000, ApJ, 541, 270
Bloemhof E. E., & Danen R. M., 1995, ApJ, 440, L93
Castro, S., et al., 2001, ApJ, 548, L197
Cassan, A., et al., 2004, A&A, 419, L1
Cassinelli, J. P., Nordsieck, K. H., Murison, M. A., 1987, ApJ, 317, 290
DiStefano R., Perna R., 1997, ApJ, 488, 55
Dominik M., 1998, A&A, 349, 108
Dominik M., 2004a, MNRAS, 352, 1315
Dominik M., 2004b, MNRAS, 353, 118
Gail, H.-P., Sedlmayr, E., 1986, A&A, 166, 225
Gaudi B. S., Gould A., 1999, ApJ, 513, 619
Gould A., 1994, ApJ, 421, 71
Gould A., 2001, PASP, 113, 903
Habing H. J., Tignon, J., Tielens, A. G. G. M., 1994, A&A, 286, 523
Hendry M. A., Coleman I. J., Gray N., Newsam, A. M., Simmons, J. F. L., 1998, New Astronomy Reviews, 42, 125.
Heyrovský D., Sasselov D., 2000, ApJ, 529, 69
Heyrovský D., Sasselov D., Loeb A., 2000, ApJ, 543, 406
Ignace R., Hendry M. A., 1999, Astron. Astrophys., 341, 201
Jorgensen U. G., Johnson H. R., 1992, A&A, 265, 168
Lamers H. J. G. L. M., Cassinelli J. P., 1999, Introduction to Stellar Winds, (Cambridge University Press)
Mao S., Paczynski B., 1991, ApJ, 374L, 37
Mao S., di Stefano R., 1995, ApJ, 440, 22
Maoz D., Gould A., 1994, ApJ, 425, 67
Nemiroff R. J., Wickramasinghe W., 1994, ApJ, 424, 21.

Netzer N., Elitzur, M., 1993, ApJ, 410, 701
Newsam, A. M. Simmons J. F. L., Hendry M. A., Coleman I. J., 1998, New AR, 42, 121.
Peng E. W., 1997, ApJ, 475, 43.
Sackett P. D., 2001, Microlensing 2000: A New Era of Microlensing Astrophysics. ASP Conf. Ser. in press (ASP: San Francisco)
Schneider P., Wagoner R. V., 1987, ApJ, 314, 154.
Schneider P., Weiss A., 1986, Astron. Astrophys, 164, 237.
Simmons J. F. L., Willis J. P., Newsam A. M., 1995a, A & A, 293, L46.
Simmons J. F. L., Newsam A. M., Willis J. P. 1995b, MNRAS, 276, 182.
Simmons J. F. L., Bjorkman J. E., Ignace R., Coleman I. J.,2002, MNRAS, 336, 501
Valls-Gabaud D., 1998, MNRAS, 294, 747.
Witt H. J, 1995, ApJ, 449, 42
Witt H. J., Mao S., 1994, ApJ, 430, 505